

## Thickness-Driven Spin Reorientation Transition in Co/Pd(111) : *In Situ* SMOKE Three-Dimensional Vector Magnetometry

Jeong-Won Lee<sup>a</sup>, Sang-Koog Kim<sup>a</sup>, Jonggeol Kim<sup>a</sup>, Jong-Ryul Jeong<sup>a</sup>, Jae-Seok Ahn<sup>b</sup>,  
and Sung-Chul Shin<sup>a</sup>

<sup>a</sup>*Department of Physics and Center for Nanospinics of Spintronic Materials,  
Korea Advanced Institute of Science and Technology,  
Taejon 305-701, Korea*

<sup>b</sup>*Department of Physics, Univ. of Seoul, Seoul 130-020, Korea*

### Abstract

We have developed a three-axis configurational *in situ* SMOKE apparatus by which three-dimensional vector magnetization reversal processes are studied for ultrathin Co films grown on a Pd (111) single crystal in the thickness range of spin-reorientation transition. This study provides a better understanding of magnetization reversal motions with the knowledge of 3 components of magnetization vector at the transition of an easy axis of magnetization from the film normal at 5 ML Co to in-plane at 6 ML Co (ML notes monolayer). For a 5.25 ML Co, it was observed that a slightly canted magnetization vector from the film normal rotated in the film plane under an applied field direction parallel to the film normal.

### 1. Introduction

Understanding of magnetization orientations in ground state and/or magnetization reversal motion remains fundamental so that investigation of three dimensional (3D) full magnetization vector is of great importance. Because spin orientations in different domains or layers of magnetic thin films are closely associated with magnetic properties such as spin-reorientation transition (SRT), giant magnetoresistance (GMR) and tunneling magnetoresistance (TMR), which are very interesting phenomena technologically applicable to very recent high-density information storage. Especially, SRT behavior has been one of very interesting subjects in ultrathin film magnetism because magnetic films having strong perpendicular magnetic anisotropy (PMA) are promising candidates as ultrahigh-density recording media.

Ultrathin Co films exhibit an enhanced PMA for a few monolayers [1,2]. The PMA is sufficient to overcome demagnetizing energy of thin films and makes spontaneous magnetization direction out-of-plane as the thickness decreases. In very recent work on SRT [3], anisotropy space of the first order ( $K_1$ ) and second order anisotropy ( $K_2$ ) constants is introduced in the framework of the anisotropy free energy in order to better understand magnetization switching behavior as a function of film thickness. This concept has predicted a metastable phase of coexistence of the in-plane and out-of-plane magnetization phases as well as a canted phase, which are dependent on a relative strength of  $K_1$  and  $K_2$ . The work motivates us to develop a 3-configurational *in situ* surface magneto-optical Kerr effect (SMOKE) system to investigate 3D full vectorial

magnetization in a ground state and the magnetization reversal processes especially in the thickness range of the spin reorientation transition of ultrathin films.

The SMOKE is a premier technique for ultrathin magnetic film study because of a monolayer sensitivity and *in situ* implementation under ultrahigh vacuum (UHV) chamber [4]. It has been widely utilized for investigation of magnetic properties such as magnetic anisotropy [5], magnetic phase transition [6], and SRT [7-9]. In our work, as a prototype, we choose Co films grown on a surface of a Pd (111) single crystal. Vector nature of magnetization reversal process is clearly identified for 5.0 – 6.0 ML Co films, where SRT occurs from out-of-plane to in-plane.

## 2. Experiments

The experiments were carried out in an ultrahigh vacuum chamber with a base pressure of  $5 \times 10^{-11}$  Torr, which was especially designed to permit 3-axis configurational *in situ* SMOKE measurements and deposition at the same position without sample transportation. Co films were grown on a single crystal Pd(111) substrate by e-beam evaporation with a deposition rate of 0.8 Å/min at room temperature. Pd(111) substrate was cleaned by several cycling of sputtering with Ar<sup>+</sup> ion of a 1 keV energy followed by annealing at 900 K. Well-formed terrace structure of the Pd(111) surface was confirmed by STM study. Details of the SMOKE measurement system were described elsewhere [10].

To investigate 3D vectorial magnetization reversals of ultrathin Co films in the thickness range where SRT occurs, we measured *in situ* Kerr rotation and ellipticity with an accuracy down to  $0.001^\circ$  through phase-sensitive detection using a precise photoelastic-modulator and crystal polarizers with extinction ratio of better than  $10^{-5}$ . The sample stage could be rotated  $\pm 60^\circ$  in the film plane with a precision manipulator, allowing various measurement geometries at different scattering planes. To obtain SMOKE data needed for a complete analysis of 3D vectorial magnetization during magnetization reversals, SMOKE signals were taken at 3 configurations as depicted in Fig. 1: (1) two polar configurations in the yz and xz scattering planes with a magnetic field applied along the film normal; (2) longitudinal configuration in the yz scattering plane with an applied field parallel to the y-axis. These three configurational measurements are sufficient to obtain SMOKE data needed for 3D vectorial determination of the magnetization directions during magnetization reversal.

## 3. Description of 3D vector magnetometry using SMOKE

Very recently, we reported a magnetization reversal process for a Co thin film represented by 3D magnetization vector motion as a function of an applied magnetic field using simplified analytic expressions for MOKE in magnetic film where an ultrathin magnetic film has an arbitrary magnetization orientation and the probing light is obliquely incident to the film plane [11,12]. When the scattering plane is located in the yz plane, complex Kerr effects for the p- and s-waves in the ultrathin limit,  $\Theta^p(M_y, M_z)$  and  $\Theta^s(M_y, M_z)$ , are given as follows:

$$\Theta^p(M_y, M_z) = \frac{\cos \theta_0}{\cos(\theta_0 + \theta_2)} \left( M_y \frac{\sin^2 \theta_1}{\sin \theta_2} + M_z \cos \theta_2 \right) \Theta_n, \quad (1-a)$$

$$\Theta^s(M_y, M_z) = \frac{\cos \theta_0}{\cos(\theta_0 - \theta_2)} \left( M_y \frac{\sin^2 \theta_1}{\sin \theta_2} - M_z \cos \theta_2 \right) \Theta_n, \quad (1-b)$$

where  $\theta_0$ ,  $\theta_1$ ,  $\theta_2$ ,  $\Theta_n$  are the incident angle, complex refractive angles of the magnetic thin film and the nonmagnetic substrate, and the complex polar Kerr angle for normal incidence in the ultrathin film limit, respectively. Here, the incident angle is  $\theta_0 = 45^\circ$ .  $M_y$  and  $M_z$  are the direction cosines of the magnetization vector in the y- and z-directions, respectively. In the case of xz scattering plane,  $M_y$  can be replaced by  $M_x$ . In general,  $\theta_1$ ,  $\theta_2$ , and  $\Theta_n$  in Eqs. (1) are sensitively dependent on the thickness and optical properties of a thin film; *in situ* determination of these values for a growing film is very difficult or at least requires another techniques such as *in situ* ellipsometry for obtaining the exact values of those for the growing films. However, it is not necessary to directly measure those values for our vectorial analysis of magnetization orientations if the saturation values of Kerr angles for each growing film can be obtained as described below. All the components,  $M_x$ ,  $M_y$ , and  $M_z$  can be determined as follows:

$$M_{x,y} = \frac{\Theta_p^s \Theta^p(M_{x,y}, M_z) - \Theta_p^p \Theta^s(M_{x,y}, M_z)}{\Theta_L^p \Theta_p^s - \Theta_p^p \Theta_L^s} \quad (2-a)$$

$$M_z = \frac{\Theta_L^s \Theta^p(M_{x,y}, M_z) - \Theta_L^p \Theta^s(M_{x,y}, M_z)}{\Theta_p^p \Theta_L^s - \Theta_L^p \Theta_p^s} \quad (2-b)$$

where,  $\Theta_i^j$  denotes the saturation values of measured complex Kerr angles for the *i*-polarization wave (*i* = s- and p-waves) in *J*-measurement configuration. Therefore, one can determine all the components of magnetization vector **M** during reversal process using simple Eqs. (2).

#### 4. Results and Discussion

Fig. 2 shows the evolution of polar and longitudinal SMOKE hysteresis loops with Co film thickness grown on a Pd(111) single crystal. For 1 ML Co no hysteresis loop appears in both geometries. This can be ascribed to the loss of ferromagnetism, consistent with a Co/Au(111) case [13], where initial ferromagnetic order appears at 1.5 ML Co. The loss of ferromagnetism in the Co monolayer on Pd(111) surface may be explained by superparamagnetism at room temperature [14]. Onset of appearance of Kerr rotation and coercivity occurs at 1.5 ML Co. Hysteresis loops and coercivities start to appear from 4 ML Co in longitudinal geometry. This is because the longitudinal coercivities of those thicknesses exceed a maximum field of 2 kOe available in our system in a range of  $1 \text{ ML} < t_{\text{Co}} < 4 \text{ ML}$  as evident from the trend of the longitudinal

coercivity with  $t_{Co}$ . Generally, the longitudinal coercivities for below 4 ML Co are much larger than polar ones and drastically decrease with the small increase of Co coverage at the transition of magnetization orientation from perpendicular to in-plane. In the thickness range of 2 ML  $\sim$  4.5 ML, the coercivities of the polar loops are about  $\sim$  100 Oe. Above 5 ML, polar hysteresis loops start to change and show a hard axis loop, while the longitudinal ones become square in shape with small coercivities. It is clear from the *in-situ* SMOKE data that SRT takes place between 5 and 6 ML Co.

In order to better understand spin switching behavior during reversal process especially in the transition region, we have measured Kerr hysteresis loops of both p- and s-waves for two polar and one longitudinal configurations for  $t_{Co} = 5, 5.25,$  and 6 ML as demonstrated in Fig. 3. These data are necessary to determine 3D magnetization vector of the film during magnetization reversal process. As described earlier, we used Eqs. (2) where each value of  $\Theta_j^i$  can be obtained from the SMOKE data shown in Fig. 3 to determine three components,  $M_x, M_y,$  and  $M_z$  of magnetization vector  $\mathbf{M}$ .

Resulting  $M_x, M_y,$  and  $M_z$  as a function of  $\mathbf{H}$  are shown in Fig. 4 along with their parametric representation on the  $xy, yz,$  and  $xz$  planes in Fig. 5. For a 5 ML Co film, a simple magnetization reversal is obtained due to strong perpendicular magnetic anisotropy as seen in Fig. 2. The magnetic fields above 90 Oe easily saturate magnetizations along the field direction along the film normal as demonstrated by scattered data points around  $M_x = M_y = 0$  in the  $xy$  projection, around  $M_z = 1, M_x = M_y = 0$  in the  $xz,$  and  $yz$  planes.

For a 5.25 ML Co film, a complex reversal motion of magnetizations is observed, which itself demonstrates a power of ability of 3D vector magnetometry using SMOKE. Both  $M_x$  and  $M_y$  components are considerable except at the high strength of magnetic field as seen in  $xy$  projection. At high fields the two components are near zero since the film is saturated to the perpendicular direction. As the applied field decreases, the two components increase. The magnetization reversal process in  $xz$  plane is irreversible, but  $yz$  projection shows a reversible behavior under the magnetic field applied to the film normal.

In a 6 ML Co film, as seen in each plane,  $M_x$  is not observed at all, but  $M_y$  is observed at low fields along the film normal. On  $yz$  plane, as the saturation field decreases  $M_z$  component decreases while  $M_y$  increases, indicating initial coherent rotation. Further decrease in the normal field forms multidomains of in-plane magnetizations, and the remanance of  $M_y$  indicates imbalance of areas of opposite directions of  $\mathbf{M}$  along  $y$ -axis. As the field increases along the negative  $z$ -direction, wall displacement of in-plane domains reduces  $M_y$  component and then, coherent rotation of in-plane magnetizations follows toward perpendicular direction.

## 5. Summary

We have studied spin-reorientation transition of ultrathin Co films grown on a Pd (111) single crystal using *in situ* SMOKE 3D vector magnetometry, which enables to determine 3D vector magnetization during reversal process. In the transition range of spin reorientation, each component of  $\mathbf{M}$  shows different reversal behaviors. For the 5.0 ML Co of perpendicular magnetization, multidomains of perpendicular magnetization are formed and switch via collective spin rotation near a coercive field. For the 6.0

ML Co of in-plane magnetization, coherent rotation of magnetization orientations occurs from perpendicular to in-plane as the saturation field decreases and then, multidomains of in-plane magnetization are formed near the coercive field. For the case of 5.25 ML, where canted magnetization phase is observed, in-plane components of  $\mathbf{M}$  rotate in the plane at a low field during reversal process. As demonstrated in this work, this method is very useful to better understand magnetization reversal processes with the aid of 3D vector representation of  $\mathbf{M}$ .

### Acknowledgements

This work was supported by the Korean Ministry of Science and Technology through the Creative Research Initiatives Program.

### References

1. R. Allenspach, *J. Magn. Magn. Mater.* **129**, 160 (1994).
2. J. Thomassen, F. May, B. Feldmann, M. Wutting, and H. Ibach, *Phys. Rev. Lett.* **69**, 3831 (1992).
3. Y. T. Millev, H. P. Oepen, and J. Kirschner, *Phys. Rev. B* **57**, 5848 (1998).
4. E. R. Moog and S. D. Bader, *Superlattice and Microstructure* **1**, 543 (1985); S. D. Bader, *J. Magn. Magn. Mater.* **100**, 440 (1991).
5. B. Heinrich and J. F. Cochran, *Adv. Phys.* **42**, 523 (1993); S. Hope, E. Gu, B. Choi, and J. A. C. Bland, *Phys. Rev. Lett.* **80**, 1750 (1998).
6. Z. Q. Qui, J. Pearson, and S. D. Bader, *Phys. Rev. Lett.* **67**, 1646 (1991); Y. Li and K. Baberschke, *Phys. Rev. Lett.* **68**, 1208 (1992).
7. Z. Q. Qiu, J. Pearson, and S. D. Bader, *Phys. Rev. Lett.* **70**, 1006 (1993).
8. A. Berger, A. W. Pang, and H. Hopster, *Phys. Rev. B* **52**, 1078 (1995).
9. M. Farle, B. Mirwald-Schulz, A. N. Anisimov, W. Platow, and K. Baberschke, *Phys. Rev. B* **55**, 3708 (1997).
10. J.-W. Lee, J.-R. Jeong, D.-H. Kim, J. S. Ahn, J. Kim, and S.-C. Shin, *Rev. Sci. Instrum.* (to be published).
11. C.-Y. You and S.-C. Shin, *Appl. Phys. Lett.* **69**, 1315 (1996); *J. Appl. Phys.* **84**, 541 (1998).
12. Sung-Chul Shin, Jeong-Won Lee, Sang-Koog Kim, and Jonggeol Kim, *Appl. Phys. Lett.*, submitted (2000).
13. R. Allenspach, M. Stampanoni, and A. Bishof, *Phys. Rev. Lett.* **65**, 3344 (1990); S. Padovani, I. Chado, F. Scheurer, and J. P. Bucher, *Phys. Rev. B* **59**, 11887 (1999).
14. J. A. C. Bland and B. Heinrich, Eds., *Ultrathin Magnetic Structures I and II*, (Springer-Verlag, Berlin, 1994).

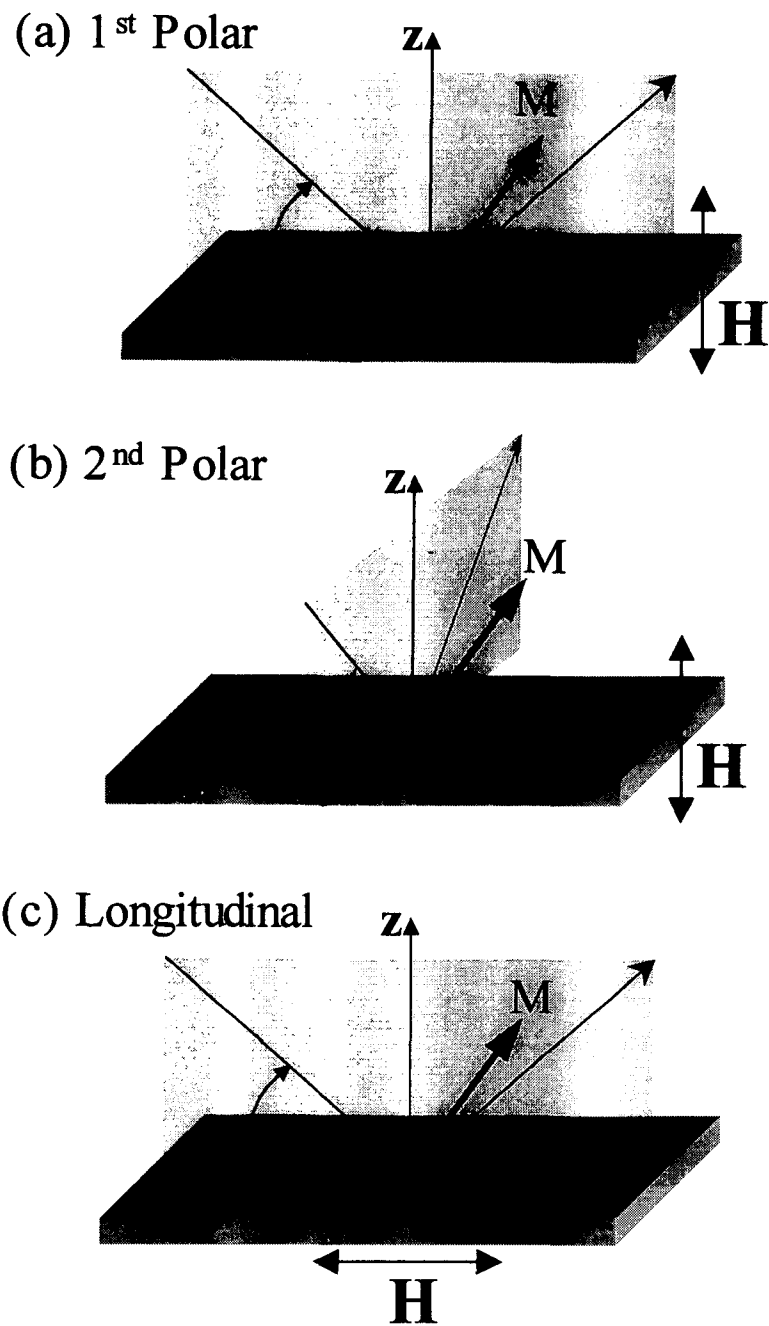


**Fig. 1.** The coordinate systems of three-axis configurations of SMOKE measurements: Polar Kerr measurements in the yz (a) and xz (b) scattering planes where a magnetic field is applied along the film normal and longitudinal measurement in the yz (c) scattering plane where the magnetic field is parallel to the y-axis.

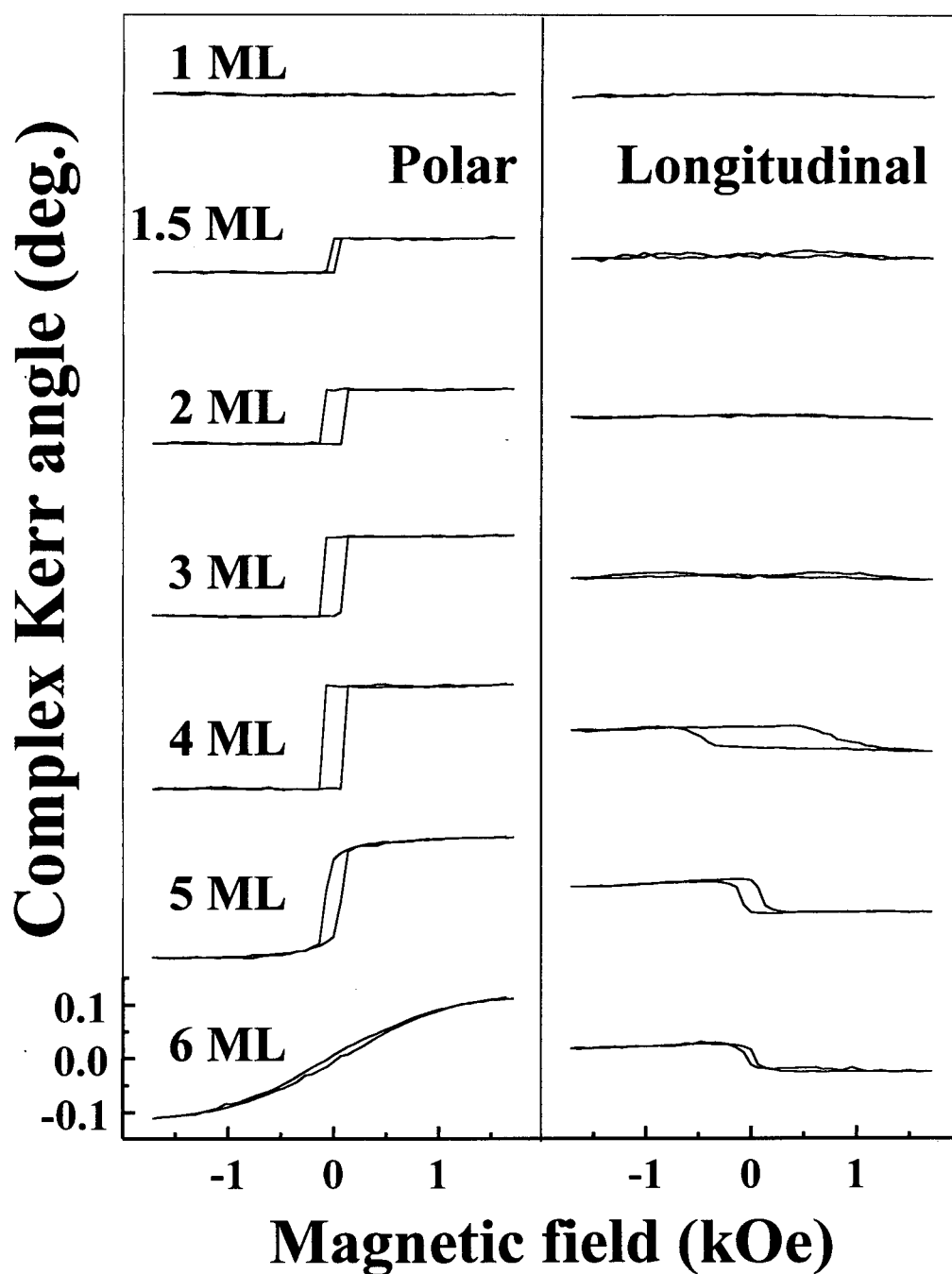


Fig. 2. Magnetic hysteresis loops measured through *in situ* polar and longitudinal Kerr effects for growing Co films on a Pd(111) single crystal. The numbers indicate the thickness of Co films,  $t_{\text{Co}}$ .

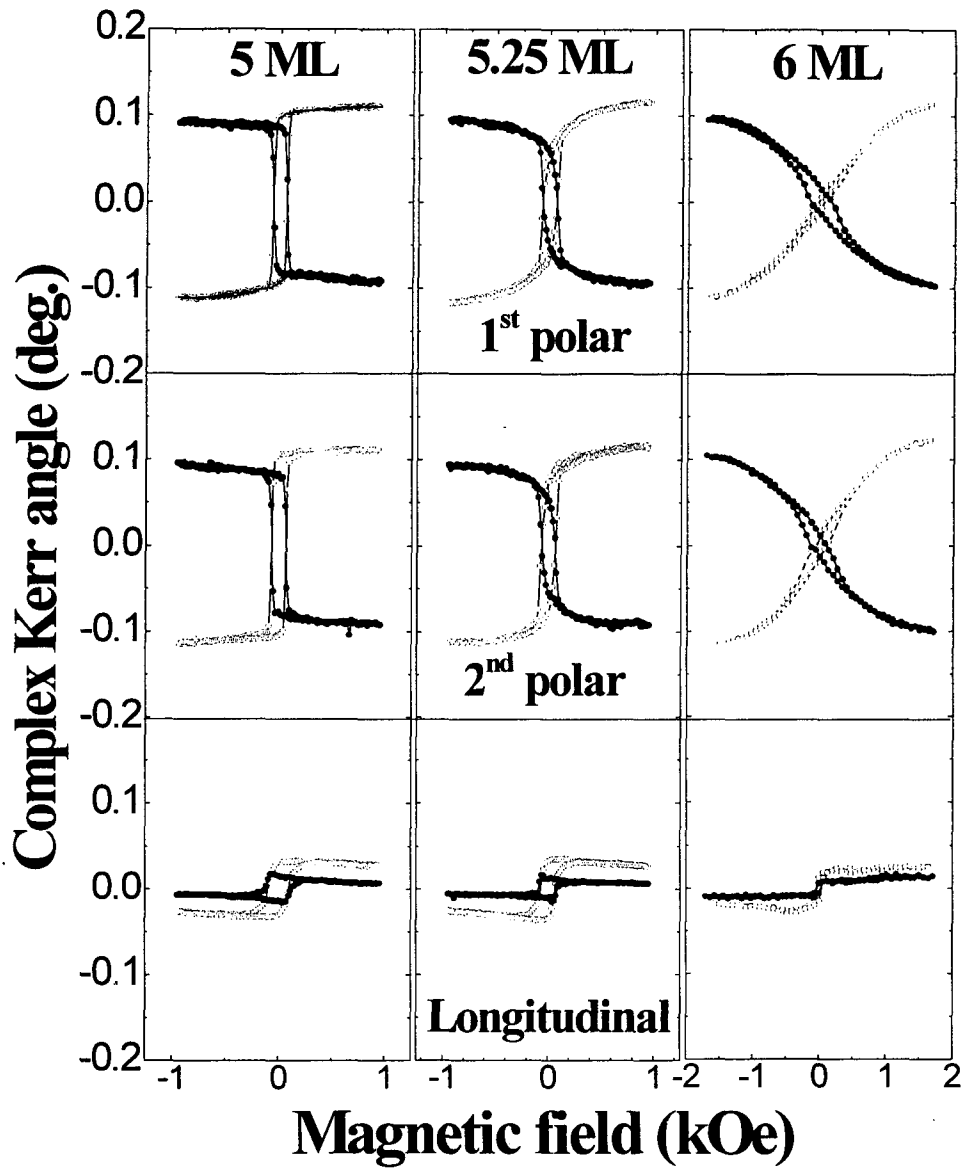


Fig. 3. SMOKE hysteresis loops measured with p-(open circles) and s-(solid circles) waves for  $t_{Co}=5.0$ , 5.25, and 6.0 ML. Each measurement configuration is described in Fig. 1.



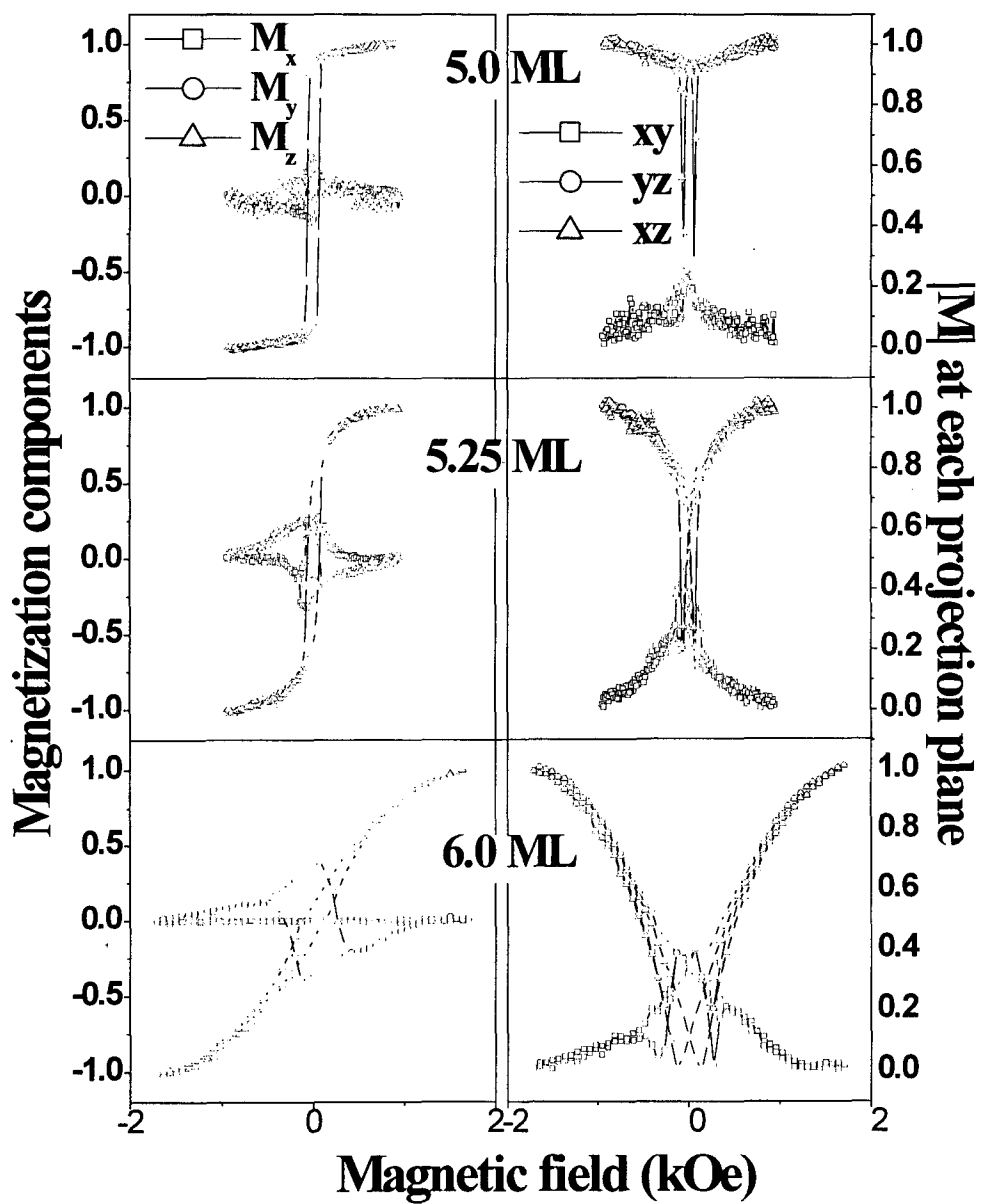


Fig. 4. Hysteresis loops of the  $M_x$ ,  $M_y$ , and  $M_z$  components of  $M$  in left panel and the magnitude of  $M$  projected on the  $xy$ ,  $yz$ , and  $xz$  planes in right panel for  $t_{Co}=5.0$ , 5.25, and 6.0 ML.

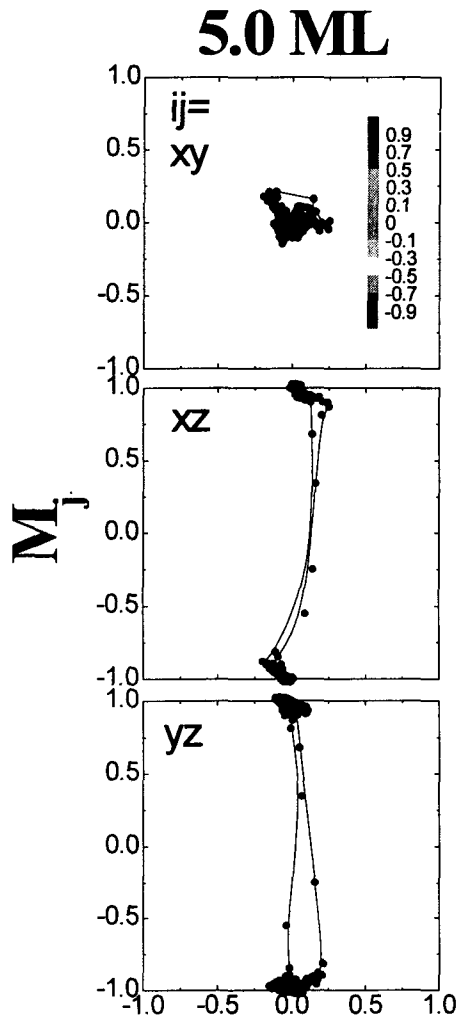


Fig. 5. 2D representations of  $\mathbf{M}$  projected on the  $xy$ ,  $yz$ , and  $xz$  plane which show 3D  $\mathbf{M}$  reversal motions. Color scaled bars indicate the strength of magnetic field applied perpendicular to the film plane. This parametric representation of  $\mathbf{M}$  is obtained from the data of  $M_x$ ,  $M_y$ , and  $M_z$  shown in Fig. 4.